Supplementary information

Detailed secondary beam characteristics from FLUKA simulations

The yield, mean energy and beam radius of all secondary species produced by the proton beam irradiation of the target are given in Table 1, obtained at the rear surface of the target. The particle spectra of electrons, positrons and protons are given as a function of relativistic Lorentz factor in Figure 1.

Species	Specified energy range	Yield (per primary)	Mean energy, $\langle E \rangle$ (GeV)	Beam radius, σ_r (mm)
e^-	≥ 1 MeV	56	0.20	2.0
e^+	≥ 1 MeV	46	0.27	1.9
p^+	≥ 100 keV, < 430 GeV	1.4	31	1.2
p^+	≥ 430 GeV	0.42	439	1.2
$\pi^\pm$	≥ 100 keV	6.2	6.6	1.7
$k^\pm$	≥ 100 keV	0.5	11	1.4
μ^-	≥ 100 keV	<0.05	-	-
γ	≥ 10 keV	600	0.07	2.0
n	≥ 100 keV	12.6	3.1	2.2

Table 1 Detailed secondary beam characteristics from FLUKA simulations. The yield (per primary), mean energy ($\langle E \rangle = \langle \Gamma \rangle mc^2$), and beam radius (half-width-half-maximum) are provided for the most abundantly produced secondary species: electrons (e^-), positrons (e^+), protons (p^+), pions ($\pi^\pm$), kaons ($k^\pm$), muons (μ^-), γ-rays and neutrons (n). The specified energy range defines the range of energies that the table parameters refer to. In the case of electrons and positrons, for ease of comparison with other studies, the low-energy cutoff used is 1 MeV, though there are even more pairs (up to 10% more) if the energy cutoff is reduced to 10 keV. For the remaining species, the low energy cutoff is defined by the simulation. The yield per primary can be multiplied by the primary proton beam intensity to obtain the actual yield. For instance, with a primary proton beam intensity of 3×10^{11} protons, a total of 1.7×10^{13} electrons and 1.4×10^{13} positrons are produced. For the muons, the simulated number is too small for reasonable statistics of the mean energy and beam radius.

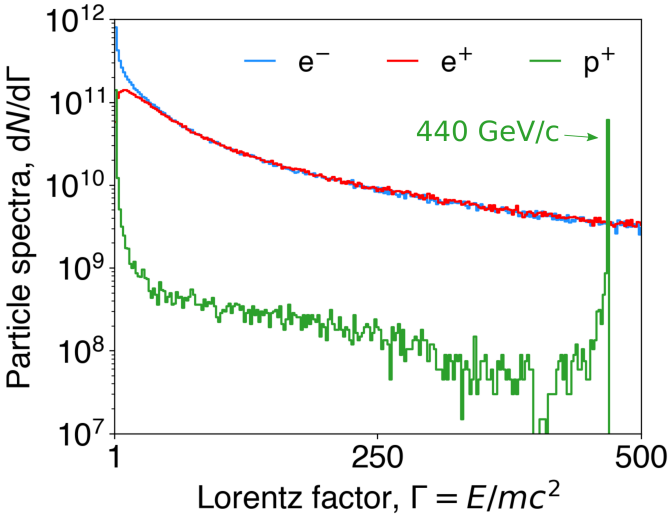

Fig. 1 FLUKA simulations of particle spectra. Particle spectra of electrons (e^-, blue), positrons (e^+, red) and protons (p^+, green) at the exit of the target are obtained from FLUKA simulations and plotted as a function of relativistic Lorentz factor, $\Gamma = E/mc^2$. The electron and positron spectra are matched except at energies $\lesssim 10$ MeV, where electrons can more easily escape the target than positrons. The e^-e^+ spectra are characterized by extended tail distribution functions with energies up to several tens of GeV. The population of primary protons which experience only elastic scattering are identified by the peak in the spectra corresponding to proton momentum $p = 440$ GeV/c.

Chromox luminescence as a function of particle type and energy

To further validate the assumption that particles deposit an approximately equal amount of energy into the screens, FLUKA simulations are performed, irradiating Chromox with different particle types and energies. The results are shown in Figure 2. In the range $2 \lesssim \Gamma \lesssim 500$, the deposited energy per particle is approximately the same across energy scales and between charged particle species. The mean energy deposited for γ-rays in the range MeV-TeV is plotted (black-dotted), showing that the energy deposition per γ-ray is approximately 300× smaller. Therefore, we expect the contribution of γ-rays to observed screen luminescence to be negligible, despite the expected yield being 6× greater than e^+e^-.

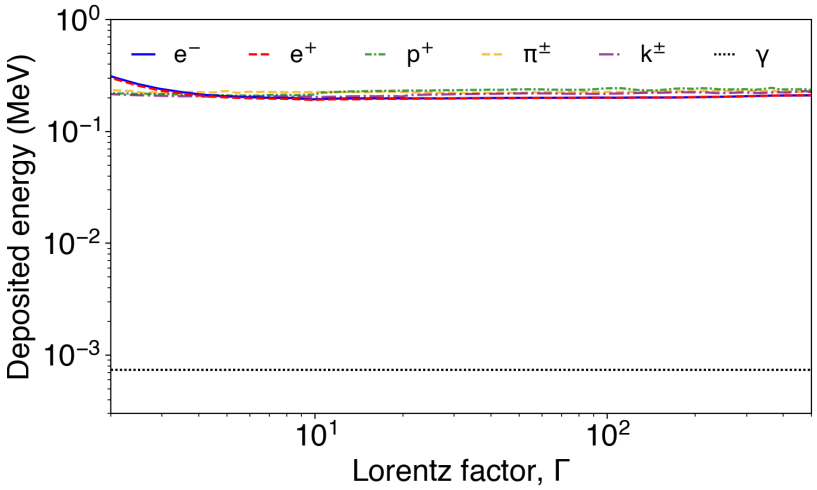

Fig. 2 FLUKA simulations of energy deposited into Chromox screens. The energy deposited per particle into a 250 µm-thickness Chromox screen at 45° incidence is obtained from FLUKA simulations. Deposited energy is plotted as a function of relativistic Lorentz factor for: electrons (e^-, blue-solid), positrons (e^+, red-dashed), protons (p^+, green-dot-dashed), charged pions ($\pi^\pm$, orange-dashed) and charged kaons ($k^\pm$, purple-dot-dashed). The mean energy deposited per γ-ray in the range MeV-TeV is also plotted (black-dotted), showing that the energy deposition of γ-rays is approximately 300× smaller.

Magnetic particle spectrometer raw data

Raw image data of the Chromox screens in the magnetic particle spectrometer is shown in Figure 3 (post-background subtraction). The increase in signal when the electromagnet is turned on is evidence of positrons in the beam with energy $E \leq 220$ MeV. The horizontal lineouts from this data in the central 25 mm are used to obtain the electron and positron spectra shown in the main text.

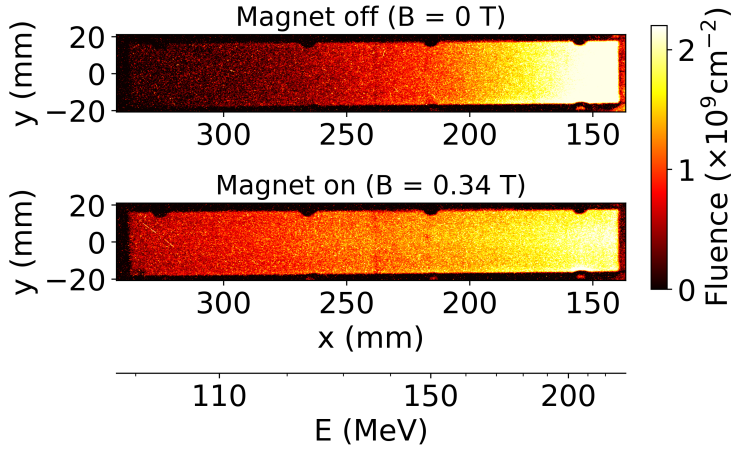

Fig. 3 Magnetic particle spectrometer raw data. Raw image data of the chromium-doped luminescence screens used to measure the energy spectra of electrons and positrons in the magnetic particle spectrometer. The screen corresponding to positrons is shown when the target is irradiated and the electromagnet is turned off (upper), and when the electromagnet is turned on with peak magnetic field $B = 0.34$ T (lower). When the magnet is turned on, positrons are deflected away from the beam axis onto the screen. The secondary x-axis shows the corresponding positron energy according to the energy calibration when the magnet is operating at the given setting.

Fitting a relativistic Maxwellian to the pair beam momentum distribution

Given that the pair plasma beams produced in this work are characterized by non-Maxwellian distribution functions, possessing relativistic thermal spreads and bulk flow ($k_{\rm B}T_{\pm} \gg m_{\rm e}c^2$), comparisons with lengthscales traditionally used to define collective behaviour in classical plasmas are done with care. The pair temperature ($T_{\pm}$) is identified as a key parameter which must be included in the consideration of the limiting scales of collective plasma processes.

We derive the screening length for a relativistically hot plasma assuming a relativistic Maxwellian (Jüttner-Synge) distribution (Eq. 4 of the main text). This screening lengthscale is analogous to the familiar Debye screening length for non-relativistic Maxwellian plasmas. Since the screening length is derived assuming zero bulk motion, to obtain the appropriate pair temperature we perform a Lorentz transformation on the FLUKA-simulated momentum spectra and fit the data to a Jüttner-Synge distribution. The number of pairs per Debye sphere is calculated in the zero-momentum frame, using the beam density and dimensions consistent with the Lorentz transformation from the laboratory frame. The fitting of the Lorentz-transformed momentum distributions is shown in Figure 4.

The number of pairs per Debye sphere is found to scale with:

$$\frac{N_{\pm}}{N_{\rm D}} \propto N_{\pm}\ {n_{\pm}}^{1/2}\ \Gamma_0^{-1/2}\ \Gamma_T^{-3/2}, \tag{1}$$

where Γ_0 is the Lorentz factor required for a transformation from the laboratory frame to the zero-momentum frame, and Γ_T is the Lorentz factor associated with the pair temperature fitted in the zero-momentum frame ($k_{\rm B}T_{\pm} = \Gamma_T m_{\rm e}c^2$).

Alternative approaches of comparing the pair beam with limiting scales of plasma collective processes do not consider the thermal spread of the beam in the screening length. Instead, a comparison is made with the plasma skin depth, using a density corresponding to a Lorentz boost to a frame co-moving with the mean pair energy ($\langle E\rangle = \langle\Gamma\rangle m_{\rm e}c^2$) [1]. There are two issues with this approach. The first is that the pair temperature is not considered, and so the treatment is as if the momentum distribution is mono-energetic at the mean particle energy. Secondly, particle spectra with extended tails can have mean Lorentz factor far-in-excess of the median Lorentz factor, therefore misrepresenting the bulk. This alternative approach leads to a different scaling for the number of particles per screening volume: $(N_{\pm}/N_{\rm D}) \propto N_{\pm}\ {n_{\pm}}^{1/2}\ \langle\Gamma\rangle^{-3/2}$. However, the approach presented in this work leads to approximately the same result if $\Gamma_0, \Gamma_T \sim \langle\Gamma\rangle^{3/4}$. Indeed this the case given $\Gamma_0 = 4.5$ and $\Gamma_T = 8$, and provided $\langle\Gamma\rangle \sim 10 - 20$, which is generally true for the laser experiments compared in Figure 4 of the main text.

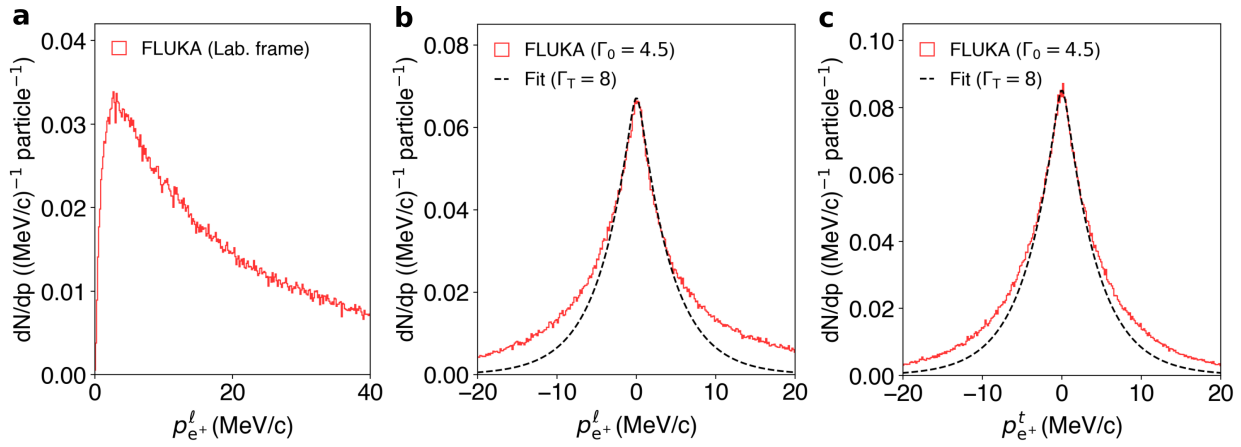

Fig. 4 Fitting the momenta distributions to relativistic Maxwellian distributions. (a) The longitudinal momentum distribution of positrons, $p^{\ell}_{\rm e^+}$, corresponding to the laboratory frame ($\Gamma_0 = 1$) is obtained from FLUKA simulations (red). (b) Once a Lorentz transformation ($\Gamma_0 = 4.5$) is applied to the particle vectors, the longitudinal momentum spectrum is modified such that it becomes approximately symmetric about zero-momentum. A relativistic Maxwellian distribution is fitted with temperature parameter $\Gamma_T = 8$ (black-dashed). (c) The transverse momentum distribution of positrons, $p^{t}_{\rm e^+}$, is plotted with the same fit.

References

[1] Chen, H. & Fiuza, F. Perspectives on relativistic electron–positron pair plasma experiments of astrophysical relevance using high-power lasers. *Physics of Plasmas* **30**, 020601 (2023).